doi:10.1006/jmbi.2000.4374 available online at http://www.idealibrary.com on IDEAL® J. Mol. Biol. (2001) 306, 97–108

JMB

Structural Basis of Diverse Sequence-dependent Target Recognition by the 8 kDa Dynein Light Chain

Jing-Song Fan, Qiang Zhang, Hidehito Tochio, Ming Li and Mingjie Zhang*

Department of Biochemistry The Hong Kong University of Science and Technology, Clear Water Bay, Kowloon, Hong Kong, P. R. China

*Corresponding author

Dyneins are multi-subunit molecular motors that translocate molecular cargoes along microtubules. Other than acting as an essential component of the dynein motor complex, the 89-residue subunit of dynein light chain (DLC8) also regulates a number of other biological events by binding to various proteins and enzymes. Currently known DLC8 targets include neuronal nitric oxide synthase; the proapoptotic Bcl-2 family member protein designated Bim; a *Drosophila* RNA localization protein Swallow, myosin V, neuronal scaffolding protein GKAP, and IκBα, an inhibitor of the NFκB transcription factor. The DLC8-binding domains of the various targets are confined within a short, continuous stretch of amino acid residues. However, these domains do not share any obvious sequence homology with each other. Here, the three-dimensional structures of DLC8 complexed with two peptides corresponding to the DLC8-binding domains of neuronal nitric oxide synthase and Bim, respectively, were determined by NMR spectroscopy. Although the two DLC8-binding peptides have entirely different amino acid sequences, both peptides bind to the protein with a remarkable similar conformation by engaging the symmetric DLC8 dimer through antiparallel β-sheet augmentation *via* the β2 strand of the protein. Structural comparison indicates that the two target peptides use different regions within the conformational flexible peptide-binding channels to achieve binding specificity. We have also re-determined the apo-form solution structure of DLC8 in this work. The structures of the DLC8/target peptide complexes, together with the dynamic properties of the protein, provide a molecular basis of DLC8's diverse amino acid sequence-dependent target recognition.

Keywords: dynein light chain; Bim; neuronal nitric oxide synthase; NMR structure; target recognition

Introduction

Cytoplasmic dynein is a multi-subunit, minus-end-directed molecular motor. It is involved in a wide range of motile events including retrograde axonal vesicle transport, membrane trafficking, spindle assembly and orientation, and nuclear migration (Hirokawa, 1998; Karki & Holzbaur, 1999; King, 2000; Vallee & Sheetz, 1996). The complex consists of two microtubule-binding heavy chains containing ATPase and motor activities (dynein heavy chain (DHC), ~500 kDa), several dynein intermediate chains (DIC, ~74 kDa) that are involved in cellular targeting, and a group of light intermediate chains (~52-61 kDa) that are thought to regulate dynein motor activity (Hughes *et al.*, 1995; Paschal *et al.*, 1992). Cytoplasmic dynein also contains several light chains (DLCs, ~8-22 kDa), whose biological functions are just beginning to be uncovered (King, 2000; King *et al.*, 1996a,b).

Unlike all other subunits that are stoichiometrically associated with the dynein complex, only a minor portion of the 8-kDa subunit of dynein light chain (DLC) (DLC8, comprising 89 amino acid residues with an actual mass of 10.3 kDa) is directly

Abbreviations used: DLC8, 8 kDa subunit of dynein light chain; nNOS, neuronal nitric oxide synthase; DHC, dynein heavy chain; DIC, dynein intermediate chain; NOESY, nuclear Overhauser enhancement spectroscopy; TOCSY, total correlated spectroscopy.

E-mail address of the corresponding author: mzhang@ust.hk

0022-2836/01/010097–12 $35.00/0

associated with dynein (King *et al*., 1996a). The majority of DLC8 is present in the cytoplasm in a non-microtubule-associated form. DLC8 is ubiquitously expressed in different cell types and is highly conserved throughout evolution, implying that the protein is likely to be a multifunctional regulatory protein (Jaffrey & Snyder, 1996; Tochio *et al*., 1998). Genetic studies showed that DLC8 is essential for the motor activity of the dynein complex since a DLC8 null mutation inhibits nuclear migration in *Aspergillus nidulans* (Beckwith *et al*., 1998). In *Drosophila*, partial loss-of-function mutations of DLC8 cause morphogenetic defects in bristle and wing development, female sterility, and disruption of sensory axon projections (Dick *et al*., 1996; Phillis *et al*., 1996), and complete loss-of-function of DLC8 is embryonic lethal *via* apoptotic events (Dick *et al*., 1996). Other than binding to molecular motors such as dynein and myosin V (Benashski *et al*., 1997), DLC8 was also found to bind to a number of other proteins and enzymes which possess diverse biological functions. For example, DLC8 binds to a 17-residue peptide fragment immediately preceding the oxygenase domain of neuronal nitric oxide synthase (Fan *et al*., 1998; Jaffrey & Snyder, 1996), although the biological significance of this interaction is not entirely clear. The protein was subsequently named PIN for the protein inhibitor of neuronal nitric oxide synthase (nNOS) (to avoid nomenclature confusion, we use DLC8 in this work in order to be consistant with the more frequently used name in the literature). Yeast two-hybrid screening identified that DLC8 can interact with the N-terminal regulatory domain of IκBα, an inhibitor of the NFκB transcription factor (Crepieux *et al*., 1997). Recently, DLC8 was found to specifically interact with Bim, a newly discovered proapoptotic Bcl-2 family protein (Puthalakath *et al*., 1999; O'Connor *et al*., 1998). In healthy cells, formation of the DLC8/Bim complex sequesters the majority of Bim to the microtubule-associated dynein complex. Upon apoptotic stimulation, the DLC8/Bim complex is released from the microtubule, and Bim is therefore freed to neutralize the anti-apoptotic activity of Bcl-2 by forming a Bim/Bcl-2 heterodimer (Puthalakath *et al*., 1999). In *Drosophila*, interaction between DLC8 and Swallow was shown to be critical for asymmetric RNA localization (Schnorrer *et al*., 2000). DLC8 was also shown to interact with the neuronal scaffold protein, GKAP. Formation of the myosin V/DLC8/GKAP ternary complex may play important roles in the trafficking of neuronal signalling complexes (Naisbitt *et al*., 2000). Inspection of the amino acid sequences of several DLC8 target proteins (e.g. nNOS, Bim, GKAP, and IκBα) reveals that the DLC8-binding regions do not share obvious amino acid sequence homology, which suggests that DLC8 is capable of binding to different targets with diverse amino acid sequences. However, the molecular mechanism of DLC8's divergent sequence recognition is essentially unknown partially due to the lack of detailed biochemical and structural studies of such interactions.

Here, we report the high-resolution solution structures of DLC8 complexed with its binding domains derived from nNOS (the nNOS peptide, comprising residues Met228 to Lys245 of nNOS) and Bim_L (48 to 56), respectively (Fan *et al*., 1998; Puthalakath *et al*., 1999). The solution structure of DLC8 complexed with the nNOS peptide is essentially identical to the recently solved X-ray structure of the protein complexed with a shorter peptide derived from nNOS (Liang *et al*., 1999). Detailed comparison of the three-dimensional structures of the complexes provides insights into the molecular basis of DLC8's diverse sequence-dependent target recognition.

Results and Discussion

Structure determination

Under the experimental conditions used in this work (pH 7.0, 30 °C, with 100 mM potassium phosphate), DLC8 forms ''dimer-of-dimer'' structures (i.e., $[DLC8/peptide]_2$) with both the nNOS peptide and the Bim peptide. In agreement with their ''dimer-of-dimer'' structure, both complexes have effective rotational correlation times of ~12 ns determined by ^{15}N-backbone relaxation studies (J.S.F. *et al*., unpublished data). The dimer-of-dimer structure of the complexes of DLC8 with the nNOS peptide and the Bim peptide, respectively, was further confirmed by analytical gel filtration chromatography and chemical cross-linking studies. Analytical gel filtration chromatography studies showed that DLC8 exists as a dimer at a protein concentration range of 0.6-5.6 mg/ml, and chemical cross-linking by disulfide bond formation also indicated that protein forms a specific dimer both in the presence and absence of target peptide (see Figure 1S in the Supplementary Materials). Only one set of resonances was observed for both DLC8 and its target peptides, indicating that both tetrameric complexes adopt symmetric dimer-of-dimer structures. Given the large effective molecular weight of the complexes (a total of approximately 210 amino acid residues), we were able to obtain complete and near complete assignments of the backbone and side-chain resonances, respectively, for DLC8 in both complexes using standard heteronuclear multidimensional NMR experiments (Bax & Grzesiek, 1993; Clore & Gronenborn, 1998). Due to the broad linewidth, initial attempts to assign resonances of the bound peptides using standard 2D ^{15}N, ^{13}C-double filtered total correlated spectroscopy (TOCSY) and nuclear Overhauser enhancement spectroscopy (NOESY) experiments on a ^{13}C,^{15}N-labeled DLC8/unlabeled peptide samples were unsuccessful. We then prepared both ^{15}N and ^{15}N, ^{13}C-uniformly labeled nNOS peptides to aid in the resonance assignment of the bound nNOS peptide. Accurate assignments of both the backbone and side-chains of the bound nNOS pep-

tide were obtained in a straightforward manner using an unlabeled DLC8/^{15}N, ^{13}C-labeled nNOS peptide sample dissolved in H_2O. The labeled nNOS peptide was also found to be particularly useful in assigning a large number of inter-molecular NOEs between DLC8 and the nNOS peptide. The NOEs obtained using unlabeled DLC8/^{15}N, ^{13}C-labeled nNOS peptide sample were further confirmed by a 3D ^{13}C F_1-filtered, F_3-edited NOESY experiments on a ^{13}C,^{15}N-labeled DLC8/unlabeled nNOS peptide sample. Assignment of the inter-DLC8 NOEs in the DLC8/nNOS peptide complex was also aided by the topology derived from the X-ray studies of apo-DLC8 (see below) and its complex with a target peptide (Liang *et al.*, 1999). The assignment of the Bim peptide signal in the DLC8 complex was also aided by using a ^{15}N-labeled peptide sample. Assignment of inter-molecular NOEs in the DLC8/Bim peptide complex was partially guided by the knowledge derived from the DLC8/nNOS peptide structure (see above). The structures of the DLC8 complexed with the nNOS peptide and the Bim peptide were determined using a total of 4430 and 4872 experimental restraints, respectively. A summary of the structural statistics are provided in Table 1, and the superimpositions of the final 20 simulated annealing structures of the both complexes are shown in Figure 1.

Overall structures of the DLC8/peptide complexes

Both DLC8/peptide complexes form compact, rectangular dimer-of-dimer structures with a 2-fold symmetry axis (Figure 2). The five β-strands from each DLC8 subunit pack with each other, forming the hydrophobic interior of the complexes. The β2-strand of each DLC8 subunit crosses over to the neighbouring subunit to form an antiparallel β-sheet with the β1-strand. Therefore, the DLC8 dimer structures represent another example of protein assembly by three-dimensional domain swapping (Schlunegger *et al.*, 1997). The extensive hydrophobic interactions between the two subunits of DLC8 (~1300 Å^2 of buried surface area between the two subunits) as well as the inter-subunit hydrogen bonds between the β-strands provide a

Table 1. Structural statistics for the family of 20 structures of the DLC8/nNOS and DLC8/Bim complexes

	nNOS	Bim
Distance restraints		
Intraresidue ($i-j=0$)	1328	1332
Sequential ($\|i-j\|=1$)	906	956
Medium range ($2 \leqslant \|i-j\| \leqslant 4$)	620	698
Long range ($\|i-j\| \geqslant 5$)	808	1220
Inter-subunit	122	150
Hydrogen bonds	184	198
Inter	230	100
Total	4198	4654
Dihedral angle restraints		
Φ	116	108
Ψ	116	110
Total	232	218
Mean r.m.s. deviations from the experimental restraints		
Distance (Å)	0.0106(±0.0006)	0.012(±0.004)
Dihedral angle (deg.)	0.0769(±0.0374)	0.04(±0.02)
Mean r.m.s. deviations from idealized covalent geometry		
Bond (Å)	0.0018(±0.0000)	0.0023(±0.0000)
Angle (deg.)	0.4041(±0.063)	0.444(±0.007)
Improper (deg.)	0.29(±0.01)	0.34(±0.01)
Mean energies (kcal mol $^{-1}$)		
E_{NOE} [a]	31.509(±1.74)	51.13(±1.11)
E_{cdih} [a]	0.071(±0.033)	0.028(±0.024)
E_{repel}	87.665(±4.34)	82.99(±3.85)
$E_{L\text{-}J}$	−769.634(±29.31)	−821.34(±20.94)
Ramachandran plot[b]		
% residues in the most favorable regions		
Residues 5 to 89 in protein	75.6	79.2
Secondary structures	82.6	84.8
Atomic r.m.s. differences (Å)[c]		
Residues 5 to 89 in protein		
Backbone heavy atoms (N, C$^\alpha$, C′ and O)	0.52	0.45
Heavy atoms	0.97	0.92

None of the structures exhibits distance violations greater than 0.3 Å or dihedral angle violations greater than 3°.

[a] The final values of the square-well NOE and dihedral angle potentials were calculated with force constants of 50 kcal mol^{-1} Å^{-1} and 200 kcal mol^{-1} rad^{-1}, respectively.

[b] The program PROCHECK (Laskowski *et al.*, 1996) was used to assess the overall quality of the structures.

[c] The precision of the atomic coordinates is defined as the average r.m.s. deviations between the 20 final structures and the mean coordinates of the protein.

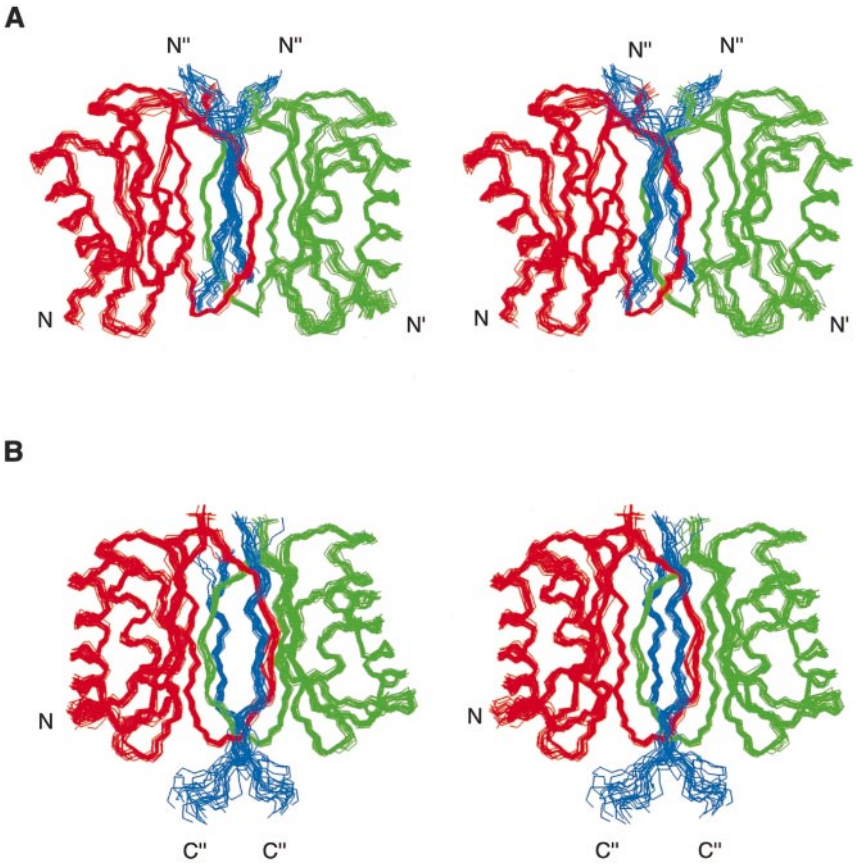

Figure 1. The solution structure of the DLC8/target peptide complexes. Stereoview showing the best-fit superposition of the backbone atoms (N, C^{α}, and C′) of the final 20 structures of DLC8 complexed with (a) the Bim peptide, and (b) the nNOS peptide. In both complexes, the structures are superimposed against the average structure using residues 5 to 89 of both subunits of DLC8 and the β-strand region of the target peptides. In both complexes, the two DLC8 subunits are shown in red and green and the target peptides are drawn in blue. For clarity, the N-terminal four residues of DLC8 are omitted in both (a) and (b). Only the N-terminal 12 residues of the nNOS peptide are shown. The N termini of the two DLC8 subunits are labeled with N and N′, respectively. The N termini of the Bim peptide are labeled with N″, and the C termini of the nNOS peptide are indicated with C″.

rationale for the observed the high stability of the DLC8 dimer structure in solution. The other face of the antiparallel β-sheet of each DLC8 monomer is packed with two amphipathic α-helices. The solvent exposed faces of the helices are enriched with charged amino acid residues, which might account for the high solubility of the complexes in solution. Table 2 lists the results of the comparison between the structures of the two complexes, and between each complex structure and the free form structure of the protein (see below). Overall, the binding of the target peptides does not induce significant conformational changes in DLC8. In particular, the β-sheet region of the protein displays an even smaller degree of target peptide-induced conformational change. The slightly larger conformational changes in DLC8 upon binding to the nNOS peptide (with respect to the binding of the Bim peptide) may reflect the fact that the nNOS peptide is longer and contains more bulky side-chains than the Bim peptide (see below for more detail). The NMR structure of the DLC8/nNOS peptide complex is very close to the X-ray structure of the protein complexed with a shorter peptide derived from nNOS (an rmsd value of 1.00 Å for residues from 5 to 89 of the protein, see Liang *et al.*, 1999).

The target peptides augment the β-sheet of DLC8 *via* the domain swapped β2 strand

The structures of the Bim peptide (residues 2 to 9) and the first 12 residues of the nNOS peptide are well defined in their respective complexes with DLC8 (Figure 1). No NOEs were observed between the last six amino acid residues of the nNOS peptide and DLC8. These six residues are likely to be dispensable in the interaction between DLC8 and the nNOS peptide. Indeed, deletion of amino acid residues up to Gly14 from the C-terminal end of

Table 2. Comparison of the structures between apo-DLC8 and its complexes with target peptides

Regions used for comparison	RMSD values (Å) apo-DLC8 *versus* DLC8/Bim peptide	apo-DLC8 *versus* DLC8/nNOS peptide	DLC8/Bim peptide *versus* DLC8/nNOS peptide
α1, α2	1.30	2.24	1.47
β0, β1, β2, β3, β4, β5	1.06	1.51	0.94
Residues 5 to 89	1.60	2.32	1.56

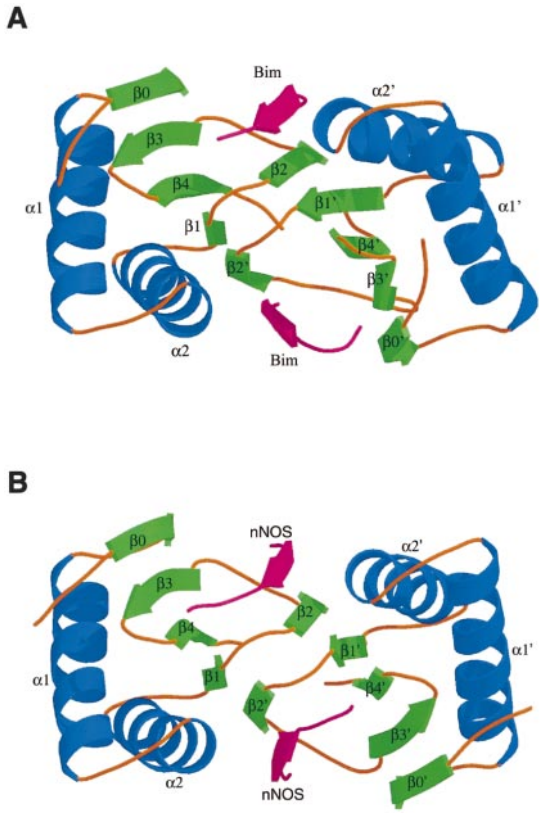

Figure 2. Ribbon diagram presentation of the DLC8/target peptide complexes. (a) and (b) The ribbon diagram structures of DLC8 complexed with the Bim peptide and the nNOS peptide, respectively. The secondary structural elements of DLC8 are labeled following the scheme of the free protein (Tochio *et al.*, 1998). The target peptides in both complexes are shown in magenta.

the nNOS peptide had no effect on its binding to DLC8 (data not shown). For clarity, we have omitted these six residues of the nNOS peptide in our structure presentation. Although the Bim peptide and the nNOS peptide share very little amino acid sequence homology with each other (Figure 3(c)), both peptides bind to DLC8 in an antiparallel β-strand fashion *via* the β2 strand of the protein (Figures 1 and 2). The amino acid residues Cys3 to Thr9 of the DLC8-bound Bim peptide assume a β-strand conformation, and residues Lys2 to Val8 in the DLC8-bound nNOS peptide adopt a β-strand structure. It should be noted that the β2 strand is involved in the domain swapping of the DLC8 dimer. At this stage, we do not understand the structural and/or functional significance of the domain swapping of DLC8. Further experiments are required in assessing both the structural and functional roles of the β2-strand mediated domain swapping of DLC8.

The peptide-binding channels of DLC8 are uniquely suited for multi-target recognition

In order to form biologically meaningful complexes, the interactions between DLC8 and its targets require an appropriate affinity and sufficient specificity. The 3D structures of the DLC8 complexes and the apo-form protein solved in this work, together with the protein's backbone dynamics both in its free and target-bound forms (J.S.F. *et al.*, unpublished data), provide insight into DLC8's diverse sequence-dependent target binding. Due to its symmetric nature, the DLC8 dimer contains two identical, concave peptide-binding channels located at the opposite sides of the dimer interface (Figure 4). Each channel is formed by the β0, β2, and β3 of one subunit and the α2 helix of the other subunit of DLC8 (Figures 2, 4 and 5). In both complexes, two molecules of the target peptides fit snugly into the target-binding channels of the DLC8 dimer. Peptide titration experiments revealed that the two peptide-binding channels do not communicate with each other (data not shown). The β2 strand serves as the base for incoming targets by forming an antiparallel β-sheet with the target peptides. The base and a large part of the peripheral areas of the channels are hydrophobic in nature (Figure 5). Yet, there are a number of polar and charged residues discretely situated at the edge of the channels. The backbone hydrogen bonds between amino acid residues from the β2 strand and the target peptides, as well as hydrophobic interactions between DLC8 and target peptides, are expected to provide favorable binding energy for the formation of the DLC8-target complexes. Polar interactions between the polar and charged amino acid residues from the channel and the target peptides are likely to play important roles in binding specificity (see below for more detail). In addition, amino acid residues in the target-binding channels (i.e. the β2 strand, the β2/β3 loop, and the α1/α2 hinge) display significant conformational exchanges at a timescale of millisecond-to-microsecond when the protein is in its apo-form (J.S.F. *et al.*, unpublished data). It is likely that the unique surface-charge potential property of the concave target-binding channels of DLC8 affords the protein the ability to form specific complexes with its target. The malleable nature of the channels further enables the protein to accommodate its targets with different amino acid sequences (therefore various shapes and sizes). Once DLC8 forms a complex with a target, the conformation of the channels becomes rigid (J.S.F. *et al.*, unpublished data). The sequence divergent interaction between DLC8 and its targets is reminiscent of the interaction between calmodulin and its targets. Calmodulin binds to several dozens of targets, and the calmodulin-binding domains of various targets share no obvious amino acid sequence homology (for a recent review, see Zhang & Yuan, 1998). The hydrophobic pockets, surrounded by negatively charged residues, and the

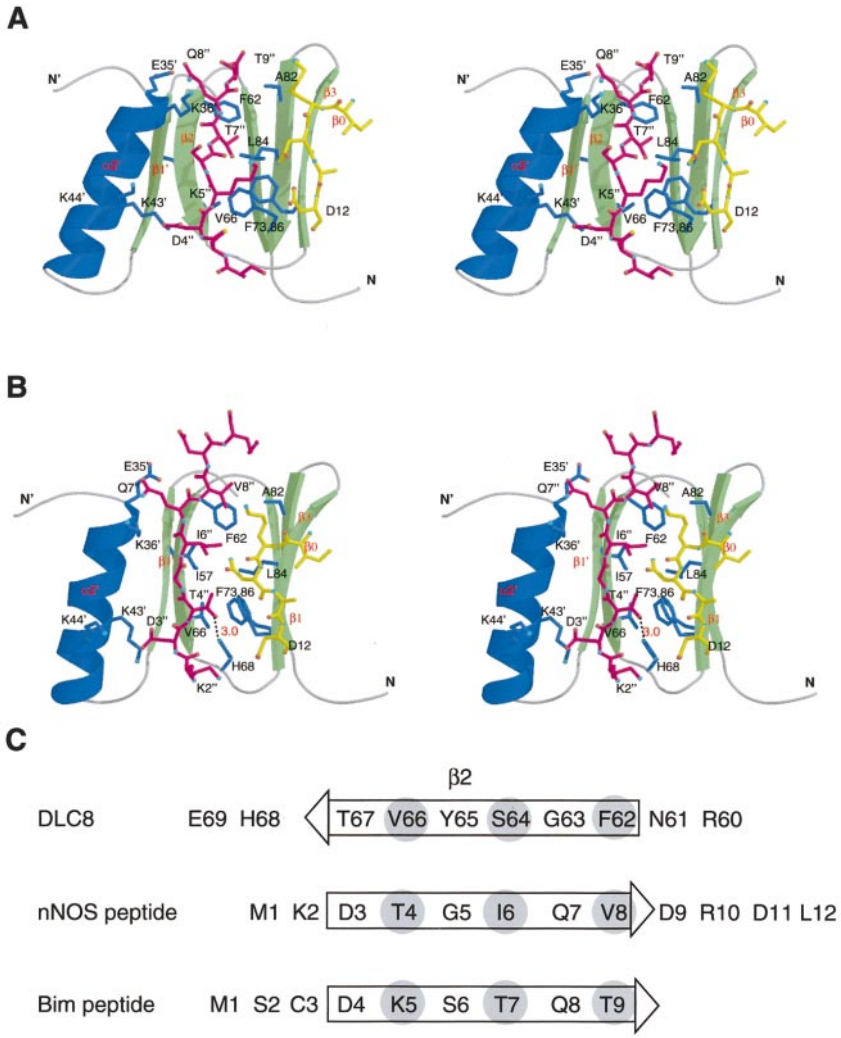

Figure 3. Comparison of the interactions of DLC8 with the Bim peptide and the nNOS peptide. Stereoview representations of (a) the Bim peptide; and (b) the nNOS peptide binding grooves of DLC8. For clarity, only the regions of DLC8 that are directly involved in the binding are included in the figure. In (a) and (b) the target peptides are shown using explicit atom representations in magenta. Amino acid residues in DLC8 that make key contacts with the peptides are also shown in the Figure. Due to its irregular strand structure, the β0 strand of DLC8 is also shown using explicit atom representations (yellow). (b) The distance between the oxygen atom of the Thr4 hydroxyl group of the nNOS peptide and the N^{ε} of His68 is also indicated. (c) Schematic showing the β-strand pairing between the β2 strand of DLC8 and the β strand of the nNOS peptide and the Bim peptide. The amino acid residues that adopt β-strand structure are highlighted by arrows. The amino acid residues in the β-strands with their side-chains pointing to the dimer interface are shaded.

flexible nature of the pockets are central to calmodulin's ability to interact with multiple targets with divergent amino acid sequences (Lee *et al.*, 2000; Zhang & Yuan, 1998).

Comparison of target peptide binding

Based on the structures of the two complexes, we have summarized the main features of the interaction between DLC8 and its target peptides. It is clear that the DLC8 target peptides are capable of forming a β-strand structure antiparallel to the existing β-sheet of DLC8 (Figure 2). Hydrogen bonds formed between the backbones of the peptide and β2 of DLC8 presumably can maintain the extended peptide conformation as well as increase the affinity of the interaction. However, an extended β-strand structure, with main interactions located within the backbones of the peptide and DLC8, does not confer the sequence-specific recognition. Therefore, the specific interaction between DLC8 and its targets must involve other regions of the protein and the peptides.

Interactions common to both target peptides

Figure 3(c) shows a schematic diagram of the β-strand pairing between the β2 strand of DLC8 and the two target peptides. Other than the Asp in the first residue (Asp3 in the nNOS peptide, and Asp4 in the Bim peptide) and the Gln in the fifth residue (Gln7 in the nNOS peptide, and Gln8 in the Bim peptide) of the β-strands, the amino acid residues at the other positions of the target peptides, which occupy the same positions of the binding channels, have very different side-chain properties. The side-chain of the Asp residue at the beginning of the target-peptide β-strands (Asp3 of the nNOS peptide, and Asp4 of the Bim peptide) interacts with a completely conserved Lys residue at the centre of α2 helix (Lys43) of DLC8 *via* charge-charge interactions (Figures 3 and 5). It has been previously shown that mutation of Asp4 in the Bim peptide significantly decreases the binding affinity between Bim and DLC8 (Puthalakath *et al.*, 1999). The Gln residue in the fifth position of the β-strands of the two target peptides (Gln8 in the Bim peptide, and Gln7 in the nNOS peptide) forms a strong hydrogen bond with the side-chain of

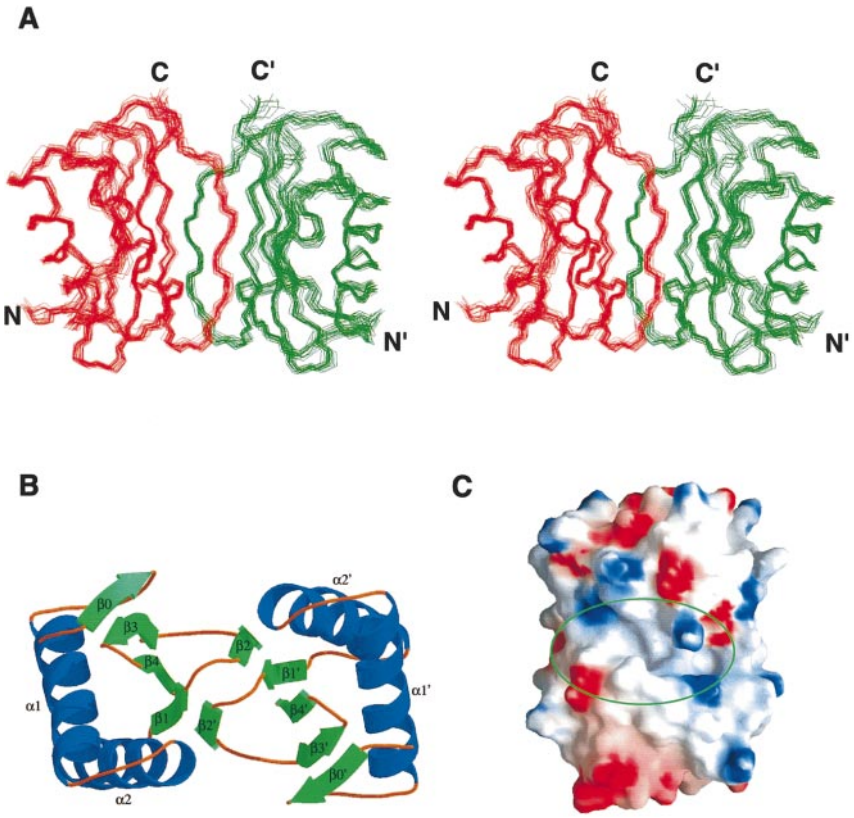

Figure 4. Solution structure of apo-DLC8. (a) Stereoview showing the best-fit superposition of the backbone atoms (N, C^{α}, and C′) of the final 20 structures of the DLC8 dimer. The structures are superimposed against the average structure using the residues 5 to 89. For clarity, the two subunits of the protein are drawn in different colors. (b) Ribbon diagram presentation of a top view of the DLC8 structure. The coloring scheme and orientation of the diagram follows those used in Figure 2. (c) Electrostatic surface potential representation of the DLC8 dimer. The molecular surfaces are colored from dark blue (most positive) to deep red (most negative) according to the local electrostatic potential on a relative scale. One of the peptide-binding channels of the DLC8 dimer is highlighted using a green oval, and the other peptide-binding channel is located on the opposite side of the molecule. The orientation of DLC8 dimer is same as the protein complexed with its target peptides (Figure 3).

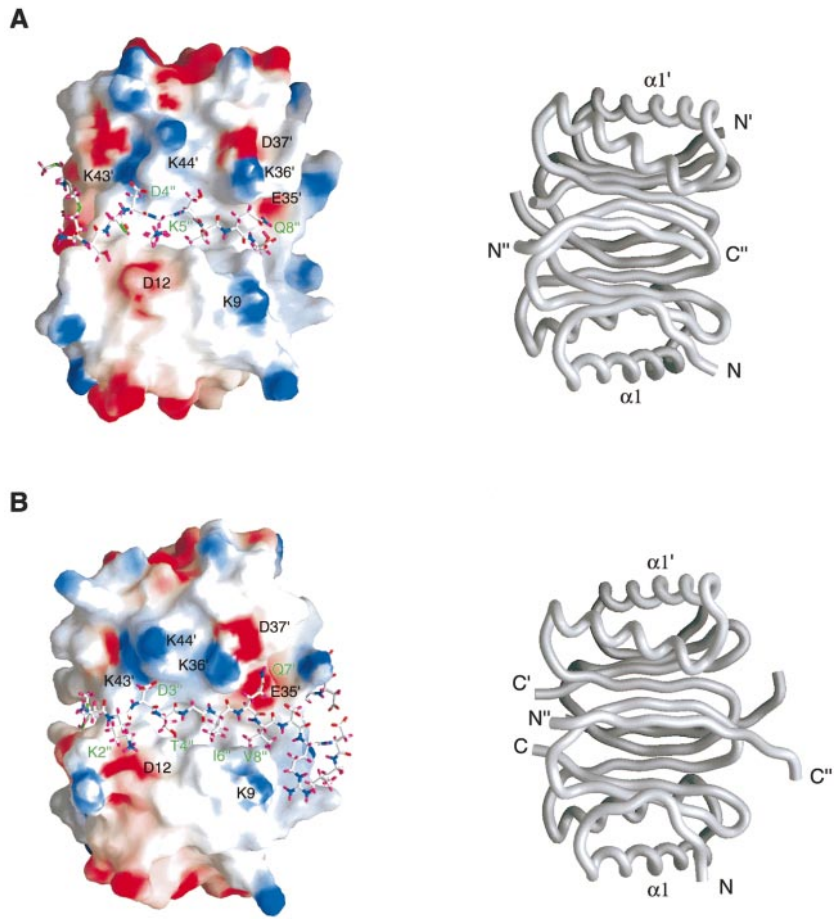

Figure 5. Target-binding grooves of DLC8. (a) and (b) The electrostatic potential surface of DLC8 complexed with the Bim peptide and the nNOS peptide, respectively. The target peptides were shown in explicit stick models, and selected amino acid residues from the peptides are labeled in green. The charged amino acid residues located within or in the vicinity of the target-binding grooves are labeled with their residue name and number (amino acid residues from different subunits of DLC8 are distinguished by a prime in their labeling). The worm models shown at the right of each surface structure are used to indicate the orientations of the complexes.

Glu35 (the first residue of α2, which is also completely conserved in different species) of DLC8 (Figures 3 and 5). The side-chain of Lys36 of DLC8 also interacts with the Gln residue from the target peptides. It is likely that the above surface charge-charge and hydrogen bonding interactions between the target peptides and DLC8 play significant roles in binding specificity.

Interactions unique to each peptide

Other than the above common side-chain interactions, the Bim peptide and the nNOS peptide use different strategies to engage DLC8. Overall, the side-chains of the Bim peptide are much less hydrophobic than those of the nNOS peptide. Lys5 in the Bim peptide is likely to play a significant role in interacting with DLC8. The aliphatic side-chain of Lys5 interacts with the aromatic amino acid residues (Phe73 and Phe86) of the protein *via* van der Waals interaction and the positively charged -$^{\varepsilon}NH_3^+$ group interacts with the negatively charged carboxyl group of Asp12 of DLC8 (Figures 3(a) and 5(a)). Mutation of Lys5 to a Glu residue completely abolished the interaction between Bim and DLC8 (Puthalakath *et al.*, 1999).

The amino acid of the nNOS peptide at the position corresponding to Lys5 of the Bim peptide is a Thr residue. During analysis of the NMR spectra of the complex, we observed many intense NOEs between side-chains of His68 in DLC8 and that of Thr4 in the nNOS peptide, indicating that these two residues are very close to each other in the complex (data not shown). The hydrogen bond interaction between side-chains of His68 and Thr4 in the DLC8/nNOS peptide complex is reminiscent of the same hydrogen bonding in PDZ/peptide complexes (Figure 3(b); Doyle *et al.*, 1996). In the PDZ/peptide complexes, a His residue in the αB helix of the PDZ domains forms a strong hydrogen bond with a Thr/Ser residue at the −2 position of target peptides (Schultz *et al.*, 1998; Songyang *et al.*, 1997). Extensive structural and biochemical studies showed that such a Thr/Ser-His hydrogen bonding interaction is critical for the specific target recognition by PDZ domains (Schultz *et al.*, 1998; Songyang *et al.*, 1997; Tochio *et al.*, 1999). Therefore, we reasoned that the same interaction seen between His68 of DLC8 and Thr4 of the nNOS peptide is also important for specific target recognition by DLC8. To test this hypothesis, we mutated Thr4 of the nNOS peptide into Ser and Gly and assayed the binding activities of the mutant GST-nNOS peptide fragments to DLC8 (Figure 6). Mutation of Thr4 into a Ser residue had no obvious effect on the peptide binding to DLC8, presumably due to the fact that the hydroxyl group of the Ser residue can still form a hydrogen bond with the side-chain of His68. In contrast, substitution of the Thr with a Gly residue significantly reduced binding affinity of the nNOS peptide to DLC8 (Figure 6). In the DLC8/nNOS peptide complex, Asp12 of the protein is also involved in the interaction with a Lys residue (Lys2) of the peptide.

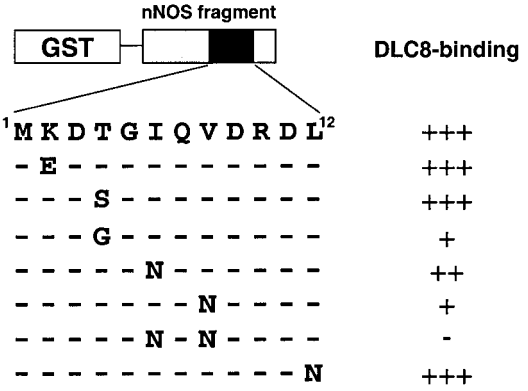

Figure 6. Identification of critical amino acid residues in the nNOS peptide for DLC8 binding. The amino acid sequence of the DLC8-binding region of the nNOS peptide (residues 1 to 12) is shown in the first row. Each mutation prepared in this study is shown in the subsequent rows. The DLC8-binding assay results, derived from the ''pull-down'' experiments, are shown at the right side of the Figure.

In addition to the formation of the antiparallel β-sheet with DLC8 by the nNOS peptide and the specific His68 to Thr4 hydrogen bonding interaction, the hydrophobic amino acid residues in several positions of the nNOS peptide are also important for the high affinity binding between DLC8 and the peptide. Substitution of Ile6 or Val8 in the nNOS peptide with a polar Asn residue significantly decreases the binding affinity between DLC8 and the GST-nNOS peptide fragment (Figure 6). Mutation of both hydrophobic residues to Asn completely abolishes the binding of the nNOS peptide to DLC8 (Figure 6). In the complex structure, both Ile6 and Val8 of the nNOS peptide intimately interact with side-chains of Ile57, Phe62, Phe73, Ala82, Leu84 and Phe86 of DLC8. Mutation of Ile6 and Val8 of the nNOS peptide is likely to disturb such hydrophobic interactions. The DLC8/nNOS peptide structure shows that Leu12 of the peptide is also involved in hydrophobic interactions with residues at the beginning of β4. However, this hydrophobic interaction does not play a critical role in the formation of the peptide-protein complex, as mutation of Leu12 to Asn has little effect on the peptide binding affinity (Figure 6).

The equivalent amino acid residues in the Bim peptide, with respect to Ile6 and Val8 of the nNOS peptide, are two Thr residues. It is expected that the hydrophobic interactions between the Bim peptide and DLC8 involving these two amino acid residues are considerably weaker than those observed in the DLC8/nNOS complex. Reverse yeast two-hybrid studies showed that mutation of Thr7 to a hydrophobic residue such as Ala or Ile disrupts the interaction between DLC8 and Bim, suggesting that

the hydroxyl group rather than the methyl group of Thr7 plays an important role in binding to the protein (Puthalakath *et al*., 1999). It is unfortunate that we were unable to define the exact role of the side-chain of Thr7 based on our structure, as no obvious interaction partner for the hydroxyl group of Thr7 can be identified in the structure. Further experiments are required to identify the exact role of Thr7 and Thr9 in mediating specific interaction between Bim and DLC8.

Solution structure of apo-DLC8 dimer

In order to resolve differences between the previously solved apo-DLC8 solution structure (Tochio *et al*., 1998) and the crystal structure of DLC8 complexed with a short peptide (Liang *et al*., 1999), we have re-determined the solution structure of the protein under slightly different sample conditions. We found that DLC8 was prone to aggregation under the condition (pH 6.0, in the presence of low concentrations of DTT) used for previous NMR structure determination (Tochio *et al*., 1998). Instead, the protein was stable for months when the pH value of the NMR samples was raised to 7.0. Excess amounts of DTT were found to be helpful in preventing disulfide-mediated protein aggregation during NMR experiments. Therefore, all NMR samples were prepared at pH 7.0 in 100 mM potassium phosphate buffer. The solution structure of the dimeric DLC8 was determined using a total of 3884 experimental restraints derived from NMR spectroscopy, including 154 inter-subunit NOEs and 12 inter-subunit hydrogen bonds (deposited in the PDB with the access code of 1F3C). The overall backbone precision for the structural ensembles shown in Figure 4(a) is 0.52 Å for the ordered regions of the dimer (including residues 5 to 89 of both subunits).

Each monomer of DLC8 contains five antiparallel β-strands (β0 in the N terminus and β1-4 in the C-terminal half of the protein), and two α-helices (α1 and α2) (Figure 4(b)). The amino acid residues from the β0, β3, the β2/β2 linker of the same subunit, and residues from the beginning of α2 in the neighboring subunit, form the peripherals of the channel. The base of each channel is largely hydrophobic, and the channel rim is surrounded by polar and charged residues (Figure 4(c)). The previously determined NMR structure of the single subunit DLC8 (PIN) differs from the currently determined structure in that the β1 and β2 strands form an intra-subunit antiparallel β-sheet structure (Tochio *et al*., 1998). Otherwise, the two-monomer structures are nearly identical. The intra-subunit antiparallel β-sheet topology of DLC8 reported earlier likely results from a misinterpretation of our chemical cross-linking data. Since DLC8 forms a highly stable dimer in solution. Extensive efforts (e.g. varying the pH of the protein sample from 5 to 10, increasing sample temperature to as high as 50 °C for a prolonged time at a very diluted protein concentration) to promote the dissociation of the protein dimer were not successful (as assessed by ^{13}C-filtered NOESY experiments). In an effort to determine the intra or inter-DLC8 subunit nature of the β1, β2 strands, we created a Tyr65 to Cys mutant of DLC8 (Cys2 and Cys24 were also mutated to Ser residues to simplify the chemical cross-linking reaction). The mutant protein was subject to disulfide-bond-mediated cross-linking. The observation of a single cross-linked band migrated at a monomeric DLC8 molecular weight on SDS-PAGE led us to conclude that formation of the Cys56-Cys65 disulfide bond between the β1 and β2 strands was intra-subunit in nature. After the publication of the X-ray structure of the DLC8/nNOS peptide complex by Liang *et al*. (1999), we decided to re-determine the structure of the apo-DLC8, both by NMR spectroscopy and X-ray crystallography. In collaboration with Dr Manfred Weiss, we have been able to obtain a 1.9 Å resolution crystal structure of the DLC8 dimer, and the topology of the protein has been confirmed to be as shown in Figure 4 (M. Weiss and M.Z., unpublished data). Determination of the apo-DLC8 structure as well as the protein complex structures described in this work was partially guided by the topology shown in the X-ray crystallographic studies.

In summary, the solution structures of DLC8 complexed with two target peptides of diverse amino acid sequences show that the protein can bind readily to a short stretch (approximately ten amino acid residues) of continuous peptide fragments using two symmetric grooves located at the dimer interface. The target peptides bind to the protein in an antiparallel β-strand fashion *via* the β2-strand of DLC8. Both polar/charge-charge and hydrophobic interactions between amino acid side-chains of DLC8 and its target peptides contribute to the specificity of binding. The conformational flexibility of the target-interacting groove confers on the protein the ability to interact with various targets possessing diverse amino acid sequences without compromising the binding affinity and specificity. The target interaction specificity of DLC8 is further complemented by discretely situated polar amino acid residues in the target-binding grooves. As the two target-binding sites of DLC8 do not communicate with each other, the protein could in principle form ternary complexes with two different targets (in addition to binding two molecules of a same target as shown in this work). Formation of such ternary complexes can indeed be observed *in vitro* (M.Z. *et al*., unpublished data) as well as *in vivo* (Naisbitt *et al*., 2000), suggesting that DLC8 can function as an adaptor molecule to link dynein with target proteins to be transported by the motor complex. The ability of DLC8 to interact with peptides of diverse amino acid sequences further implies that DLC8 may be able to bridge multiple cellular proteins to molecule motors including dynein and myosin V.

Materials and Methods

Sample preparation

Preparation of unlabeled and different forms of labeled rat DLC8 was described in detail previously (Fan *et al.*, 1998; Tochio *et al.*, 1998). The unlabeled, 18-residue nNOS peptide (MKDTGIQVDRDLDGKSHK) was commercially synthesized and HPLC purified to >95% homogeneity (Fan *et al.*, 1998). The ^{15}N and ^{15}N,^{13}C-uniformly labeled nNOS peptide was prepared by fusing the peptide together with a carrier protein thioredoxin, and the fused protein was expressed in *Escherichia coli* cells grown in M9 medium using $^{15}NH_4Cl$ and $^{15}NH_4Cl/^{13}C_6$-glucose as sole nitrogen and nitrogen/carbon sources, respectively. The labeled peptide was then cleaved from the carrier protein by protease digestion and purified by reverse phase HPLC to homogeneity (details available from the authors). The resulting labeled peptide contains five amino acid residues ($G_{-5}S_{-4}A_{-3}M_{-2}A_{-1}$) in the N terminus carried over as a cloning artefact. NMR titration studies showed that these extra five residues in the N terminus of the nNOS peptide do not affect the interaction between DLC8 and the peptide. The 9-residue Bim peptide (MSCDKSTQT) was also commercially obtained. The ^{15}N-labeled Bim peptide containing two additional residues in its N terminus ($Gly_{-2}Ser_{-1}$) was prepared in a similar manner as described above for the preparation of the stable isotope-labeled nNOS peptide.

All NMR samples were dissolved in 100 mM potassium phosphate buffer, pH 7.0 containing 10 mM d_{10}-DTT in 90% H_2O/10% ^2H_2O or 99.99% ^2H_2O. The concentrations of the NMR samples were approximately 1.5 mM of the DLC8 monomer. A total of eight NMR samples were prepared for structure determination of the DLC8/nNOS peptide complex (unlabeled DLC8/unlabeled peptide in ^2H_2O; ^{15}N-labeled DLC8/unlabeled peptide in H_2O; ^{15}N,^{13}C-labeled DLC8/unlabeled peptide in H_2O and ^2H_2O; 10% fractionally ^{13}C-labeled DLC8/unlabeled peptide in ^2H_2O; unlabeled DLC8/^{15}N-labeled peptide in H_2O; unlabeled DLC8/^{15}N,^{13}C-labeled peptide in H_2O and ^2H_2O). Six NMR samples were prepared for the structural determination of the DLC8/Bim peptide complex (except for the two doubly labeled Bim peptide/DLC8 samples, all other samples were similar to those listed for the DLC8/nNOS peptide complex structure determination).

NMR spectroscopy

All NMR experiments were performed at 30 °C on four-channel Varion Inova 500 MHz and 750 MHz spectrometers each equipped with an actively *z*-gradient shielded triple resonance probe. NMR spectra were processed with the NMRPipe software package (Delaglio *et al.*, 1995) and analyzed with PIPP (Garrett *et al.*, 1991). Sequential backbone resonance assignments were obtained by standard heteronuclear correlation experiments including HNCACB, CBCA(CO)NH, HNCO and (HB)CBCACO(CA)HA. The non-aromatic side-chain assignments were obtained using HCCH-TOCSY experiments (Bax & Grzesiek, 1993; Clore & Gronenborn, 1998). Due to the broad linewidth of the bound peptide signals, we prepared an unlabeled DLC8/^{15}N-labeled nNOS peptide, and an unlabeled DLC8/^{15}N,^{13}C-labeled nNOS peptide complex samples for unambiguous assignment of the bound peptide resonances. The resonances of the bound peptide were assigned using the same strategy as described for labeled DLC8. Stereospecific assignments of the methyl groups of Val and Leu of DLC8 in both complexes were achieved using a 10% fractionally ^{13}C-labeled DLC8 sample complexed with the two peptides (Neri *et al.*, 1989). Aromatic protons were assigned using 2D ^1H-NOESY and ^1H-TOCSY spectra of the unlabeled complex in ^2H_2O. The backbone coupling constants ($^3J_{NH\alpha}$) of DLC8 were measured using an HNHA experiment (Vuister & Bax, 1993). NOEs restraints were obtained from 2D ^1H-, 3D ^{15}N-edited, ^{13}C-edited, and ^{13}C F_1-filtered, F_3-edited NOESY spectra (Bax & Grzesiek, 1993; Clore & Gronenborn, 1998). A large number of intermolecular NOEs were also obtained from 3D ^{15}N-edited, ^{13}C-edited NOESY spectra of ^{15}N, and ^{15}N, ^{13}C-labeled peptide/unlabeled DLC8 complexes. The assignment of some inter-DLC8 subunit NOEs was also guided by the apo-DLC8 structure and the X-ray structure of DLC8 complexed with a short peptide (Liang *et al.*, 1999).

Structural calculation

The interproton distances derived from the NOE data and dihedral angle restraints were categorized as described previously (Tochio *et al.*, 1999). Hydrogen bond restraints were generated by a combination of backbone amide exchange experiments and the standard secondary structure of the protein based on NOE patterns. The NMR structures were calculated using the program CNS (Brünger *et al.*, 1998). The calculated structures were assessed with PROCHECK-NMR (Laskowski *et al.*, 1996).

Site-directed mutagenesis

GST-fused nNOS fragment, encompassing amino acid residues 161 to 245, was prepared as previously described (Fan *et al.*, 1998). The DLC8-binding region of nNOS is located at the C-terminal 17 residues of the fusion protein. All point mutations within the DLC8-binding region of the GST-fused nNOS fragment and DLC8 were generated using a PCR-based approach (Mikaelian & Sergeant, 1992). Mutant GST-fused nNOS fragments were purified using a GSH-Sepharose affinity column (Amersham Pharmacia Biotech) following the instructions of the manufacturer.

DLC8 binding assays of the nNOS fragment point mutants

The binding between DLC8 and various point mutations of the GST-nNOS fragment was assayed in 100 mM sodium phosphate buffer containing 1 mM DTT (pH 7.5). Equal molar amounts of DLC8 and various GST-nNOS fragment samples (0.8 nmol each) were mixed in 50 µl of assay buffer. The DLC8/GST-fusion protein complexes were pelleted by 10 µl of fresh GSH-Sepharose beads. The pellets were washed three times with 300 µl of assay buffer and then boiled with 30 µl of the 2 × SDS-PAGE sample buffer. The intensity of the DLC8 band on SDS-PAGE gels was used to judge the binding between DLC8 and each individual mutant of the GST-nNOS fragment.

Illustrations

The Figures were prepared using programs MOLMOL (Koradi *et al.*, 1996), MOLSCRIPT (Kraulis, 1991),

Raster3D (Merritt & Murphy, 1994), and GRASP (Nicholls, 1992). One Figure (see Supplementary Material) showing the formation of DLC8 dimer both in the absence and presence of target peptide using analytical gel filtration chromatography and chemical cross-linking studies.

Protein Data Bank Coordinates

The coordinates of the DLC8/Bim peptide and the DLC8/nNOS peptide complex structures have been deposited in the RCSB Protein Data Bank (accession code 1F95 and 1F96, respectively). The PDB accession code of the apo-DLC8 dimer structure is 1F3C. All three structural coordinates will be released upon publication of the work.

Acknowledgments

We thank Dr J. H. Wang for numerous insightful discussions during various stages of this project, Dr L. E. Kay for providing NMR pulse sequences, and Drs David Banfield and David Miller-Martini for critical reading of the manuscript. This research was supported by the RGC grants from the Research Grant Council of Hong Kong (HKUST6084/98 M, 6198/99 M, 6207/00 M). The NMR spectrometers used in this work were purchased using funds donated to the Biotechnology Research Institute of HKUST by the Hong Kong Jockey Club.

References

Bax, A. & Grzesiek, S. (1993). Methodological advances in protein NMR. *Acc. Chem. Res.* **26**, 131-138.

Beckwith, S. M., Roghi, C. H., Liu, B. & Ronald Morris, N. (1998). The ''8-kD'' cytoplasmic dynein light chain is required for nuclear migration and for dynein heavy chain localization in Aspergillus nidulans. *J. Cell. Biol.* **143**, 1239-1247.

Benashski, S. E., Harrison, A., Patel-King, R. S. & King, S. M. (1997). Dimerization of the highly conserved light chain shared by dynein and myosin V. *J. Biol. Chem.* **272**, 20929-20935.

Brünger, A. T., Adams, P. D., Clore, G. M., DeLano, W. L., Gros, P. & Grosse-Kunstleve, R. W., *et al*. (1998). Crystallography & NMR system: a new software suite for macromolecular structure determination. *Acta Crystallog. sect. D Biol. Crystallog.* **54**, 905-921.

Clore, G. M. & Gronenborn, A. M. (1998). Determining the structures of large proteins and protein complexes by NMR. *Trends Biotechnol.* **16**, 22-34.

Crepieux, P., Kwon, H., Leclerc, N., Spencer, W., Richard, S., Lin, R. & Hiscott, J. (1997). I kappaB alpha physically interacts with a cytoskeleton-associated protein through its signal response domain. *Mol. Cell. Biol.* **17**, 7375-7385.

Delaglio, F., Grzesiek, S., Vuister, G. W., Zhu, G., Pfeifer, J. & Bax, A. (1995). NMRPipe: a multidimensional spectral processing system based on UNIX pipes. *J. Biomol. NMR,* **6**, 277-293.

Dick, T., Ray, K., Salz, H. K. & Chia, W. (1996). Cytoplasmic dynein (ddlc1) mutations cause morphogenetic defects and apoptotic cell death in *Drosophila melanogaster*. *Mol. Cell. Biol.* **16**, 1966-1977.

Doyle, D. A., Lee, A., Lewis, J., Kim, E., Sheng, M. & MacKinnon, R. (1996). Crystal structures of a complexed and peptide-free membrane protein-binding domain: molecular basis of peptide recognition by PDZ. *Cell,* **85**, 1067-1076.

Fan, J. S., Zhang, Q., Li, M., Tochio, H., Yamazaki, T., Shimizu, M. & Zhang, M. (1998). Protein inhibitor of neuronal nitric-oxide synthase, PIN, binds to a 17-amino acid residue fragment of the enzyme. *J. Biol. Chem.* **273**, 33472-33481.

Garrett, D. S., Powers, R., Gronenborn, A. M. & Clore, M. G. (1991). A common sense approach to peak picking in two-, three- and four-dimensional spectra using automatic computer analysis of contour diagrams. *J. Magn. Reson.* **95**, 214-220.

Hirokawa, N. (1998). Kinesin and dynein superfamily proteins and the mechanism of organelle transport. *Science,* **279**, 519-526.

Hughes, S. M., Vaughan, K. T., Herskovits, J. S. & Vallee, R. B. (1995). Molecular analysis of a cytoplasmic dynein light intermediate chain reveals homology to a family of ATPases. *J. Cell. Sci.* **108**, 17-24.

Jaffrey, S. R. & Snyder, S. H. (1996). PIN: an associated protein inhibitor of neuronal nitric oxide synthase. *Science,* **274**, 774-777.

Karki, S. & Holzbaur, E. L. (1999). Cytoplasmic dynein and dynactin in cell division and intracellular transport. *Curr. Opin. Cell. Biol.* **11**, 45-53.

King, S. M. (2000). The dynein microtubule motor. *Biochim. Biophys. Acta,* **1496**, 60-75.

King, S. M., Barbarese, E., Dillman, J. F., III, Patel-King, R. S., Carson, J. H. & Pfister, K. K. (1996a). Brain cytoplasmic and flagellar outer arm dyneins share a highly conserved Mr 8000 light chain. *J. Biol. Chem.* **271**, 19358-19366.

King, S. M., Dillman, J. F., III, Benashski, S. E., Lye, R. J., Patel-King, R. S. & Pfister, K. K. (1996b). The mouse t-complex-encoded protein Tctex-1 is a light chain of brain cytoplasmic dynein. *J. Biol. Chem.* **271**, 32281-32287.

Koradi, R., Billeter, M. & Wuthrich, K. (1996). MOLMOL: a program for display and analysis of macromolecular structures. *J. Mol. Graph.* **14**, 51-55.

Kraulis, P. J. (1991). MOLSCRIPT: a program to produce both detailed and schematic plots of protein structures. *J. Appl. Crystallog.* **24**, 946-950.

Laskowski, R. A., Rullmannn, J. A., MacArthur, M. W., Kaptein, R. & Thornton, J. M. (1996). AQUA and PROCHECK-NMR: programs for checking the quality of protein structures solved by NMR. *J. Biomol. NMR,* **8**, 477-486.

Lee, A. L., Kinnear, S. A. & Wand, A. J. (2000). Redistribution and loss of side-chain entropy upon formation of a calmodulin-peptide complex. *Nature Struct. Biol.* **7**, 72-77.

Liang, J., Jaffrey, S. R., Guo, W., Snyder, S. H. & Clardy, J. (1999). Structure of the PIN/LC8 dimer with a bound peptide. *Nature Struct. Biol.* **6**, 735-740.

Merritt, E. & Murphy, M. (1994). Raster3D Version 2.0: a program for photorealistic molecular graphics. *Acta Crystallog. sect. D,* **50**, 869-873.

Mikaelian, I. & Sergeant, A. (1992). A general and fast method to generate multiple site directed mutations. *Nucl. Acids Res.* **20**, 376.

Naisbitt, S., Valtschanoff, J., Allison, D. W., Sala, C., Kim, E. & Craig, A. M., *et al*. (2000). Interaction of the postsynaptic density-95/Guanylate kinase domain-associated protein complex with a light

chain of myosin-V and dynein. *J. Neurosci.* **20**, 4524-4534.
Neri, D., Szyperski, T., Otting, G., Senn, H. & Wuthrich, K. (1989). Stereospecific nuclear magnetic resonance assignments of the methyl groups of valine and leucine in the DNA-binding domain of the 434 repressor by biosynthetically directed fractional 13C labeling. *Biochemistry,* **28**, 7510-7516.
Nicholls, A. (1992). *GRASP: Graphical Representation and Analysis of Surface Properties*, Columbia University, New York.
O'Connor, L., Strasser, A., O'Reilly, L. A., Hausmann, G., Adams, J. M., Cory, S. & Huang, D. C. (1998). Bim: a novel member of the Bcl-2 family that promotes apoptosis. *EMBO J.* **17**, 384-395.
Paschal, B. M., Mikami, A., Pfister, K. K. & Vallee, R. B. (1992). Homology of the 74-kD cytoplasmic dynein subunit with a flagellar dynein polypeptide suggests an intracellular targeting function. *J. Cell. Biol.* **118**, 1133-1143.
Phillis, R., Statton, D., Caruccio, P. & Murphey, R. K. (1996). Mutations in the 8 kDa dynein light chain gene disrupt sensory axon projections in the *Drosophila* imaginal CNS. *Development,* **122**, 2955-2963.
Puthalakath, H., Huang, D. C., O'Reilly, L. A., King, S. M. & Strasser, A. (1999). The proapoptotic activity of the Bcl-2 family member Bim is regulated by interaction with the dynein motor complex. *Mol. Cell.* **3**, 287-296.
Schlunegger, M. P., Bennett, M. J. & Eisenberg, D. (1997). Oligomer formation by 3D domain swapping: a model for protein assembly and misassembly. *Advan. Protein Chem.* **50**, 61-122.
Schnorrer, F., Bohmann, K. & Nusslein-Volhard, C. (2000). The molecular motor dynein is involved in targeting swallow and bicoid RNA to the anterior pole of drosophila oocytes. *Nature Cell Biol.* **2**, 185-190.
Schultz, J., Hoffmuller, U., Krause, G., Ashurst, J., Macias, M. J. & Schmieder, P., *et al*. (1998). Specific interactions between the syntrophin PDZ domain and voltage-gated sodium channels. *Nature Struct. Biol.* **5**, 19-24.
Songyang, Z., Fanning, A. S., Fu, C., Xu, J., Marfatia, S. M. & Chishti, A. H., *et al*. (1997). Recognition of unique carboxyl-terminal motifs by distinct PDZ domains. *Science,* **275**, 73-77.
Tochio, H., Ohki, S., Zhang, Q., Li, M. & Zhang, M. (1998). Solution structure of a protein inhibitor of neuronal nitric oxide synthase. *Nature Struct. Biol.* **5**, 965-969.
Tochio, H., Zhang, Q., Mandal, P., Li, M. & Zhang, M. (1999). Solution structure of the extended neuronal nitric oxide synthase PDZ domain complexed with an associated peptide. *Nature Struct. Biol.* **6**, 417-421.
Vallee, R. B. & Sheetz, M. P. (1996). Targeting of motor proteins. *Science,* **271**, 1539-1544.
Vuister, G. W. & Bax, A. (1993). Quantitative J correlation: a new approach for measuring homonuclear threebond J(HNHa) coupling constants in 15N-enriched proteins. *J. Am. Chem. Soc.* **115**, 7772-7777.
Zhang, M. & Yuan, T. (1998). Molecular mechanisms of calmodulin's functional versatility. *Biochem. Cell. Biol.* **76**, 313-323.

Edited by P. E. Wright

(Received 3 July 2000; received in revised form 18 September 2000; accepted 30 November 2000)

http://www.academicpress.com/jmb

Supplementary material for this paper comprising one Figure is available from IDEAL